Measurement 116 (2018) 483–494

Contents lists available at ScienceDirect

Measurement

journal homepage: www.elsevier.com/locate/measurement

Broadband acoustic local positioning system for mobile devices with multiple access interference cancellation

Teodoro Aguilera[a,*], Fernando Seco[b], Fernando J. Álvarez[a], Antonio Jiménez[b]

[a] Sensory Systems Research Group (GISS), University of Extremadura, E-06006 Badajoz, Spain
[b] Localization and Exploration for Intelligent Systems Group (LOPSI), Centre for Automation and Robotics (CSIC-UPM), Ctra. de Campo Real km 0.200, E-28500 Arganda del Rey (Madrid), Spain

ARTICLE INFO

Keywords:
Acoustic localization systems
CDMA signal processing
Mobile devices

ABSTRACT

This paper presents an Acoustic Local Positioning System (ALPS) suitable for indoor localization of mobile devices, based on the transmission of high frequency Code Division Multiple Access (CDMA) audio signals from a fixed beacon network to a tablet computer. The system permits positioning of the device (and the user carrying it) within a few centimeters, which is accurate enough for most location-based applications. It also implements a CDMA scheme for localization, including compensation for the limited transmission frequency band of the sensors which causes Intersymbol Interference (ISI), as well as Multiple Access Interference (MAI) between the different beacons. Signal reception, processing and estimation of position all take place within the tablet, operating at real time and with an update rate of 2 Hz. Experimental results show that the MAI/ISI compensation algorithm increase both the system's robustness (availability ⩾90%) and accuracy (errors ⩽10 cm) under adverse circumstances such as near-far effect or noisy conditions.

1. Introduction and related works

From the appearance of the first Local Positioning Systems (LPS) for indoor environments to the present time many technological solutions have been proposed [1–3]. Nowadays, the local positioning in indoor environments with mobile devices such as smartphones and tablets is becoming increasingly relevant. Some applications of LPS are the location, tracking and guidance of people in indoor environments, as well as new ways of interacting with the objects in their surroundings. Especially noteworthy are Location Based Services (LBS) apps which are based upon knowledge of the users location to provide them relevant information about their environment.

Currently, mobile smart devices are equipped with a large number of built-in sensors which offer various possibilities in the design of a LPS. In that sense, Pedestrian Dead Reckoning (PDR) systems [4] make use of these sensors (accelerometer, gyroscope and magnetometer) to obtain accuracies (errors respect to the final position) of about 10% of the total walked distance. To improve these results other authors propose adding extra inertial sensors carried by the user [5] or including Map-Matching techniques [6].

Of particular relevance today are location systems based on Radio Frequency (RF) since most mobile devices incorporate this technology off-the-shelf. Their positioning technique is based on the measurement of the Received Signal Strength (RSS), either from Wireless Personal Area Network (WPAN) such as Bluetooth [7], Bluetooth Low Energy (BLE) [8] and Ultra Wide Band (UWB) [9], or from Wireless Local Area Network (WLAN) such as WiFi [10] transceivers. Because of the complex propagation of RF signals indoors, RSS measurements are subject to large variability in this kind of environments, resulting in typical positioning errors between one and a few meters. This poor accuracy has been enhanced by fusing RSS measurements with the information provided by the remaining mobile sensors such as the accelerometer [11], accelerometer and the magnetometer [12], gyroscope [13], magnetometer and the gyroscope [14], barometer [15] or even using all of them [16].

On the other hand there are some LPS, as the one proposed in this work, that benefit from the low propagation speed of sound in air to achieve centimeter accuracy by measuring the Time-of-Arrival (ToA) of acoustic signals [17]. These Acoustic Local Positioning Systems (ALPS) can be easily implemented in portable devices since most of them are equipped with audio recording/emitting hardware off-the-shelf, although this hardware is not prepared to work in the medium or high frequency ultrasonic range. The frequency response of mobile devices' microphones and speakers is always below 22 kHz and their audio acquisition sampling rates are not higher than 96 kHz.

One of the first works appearing in literature, called *Beep* [18], and

* Corresponding author.
E-mail address: teoaguibe@unex.es (T. Aguilera).

https://doi.org/10.1016/j.measurement.2017.11.046
Received 15 May 2017; Received in revised form 13 November 2017; Accepted 17 November 2017
Available online 21 November 2017
0263-2241/ © 2017 Elsevier Ltd. All rights reserved.

a later evolution of this work [19], propose a centralized LPS where a Personal Digital Assistant (PDA) emitted short ultrasonic pulses that were detected by an array of six microphones, connected through a WLAN with a central process unit. These systems achieved positioning accuracies below 70 cm in 90% of cases, improving to 40 cm in positions away from walls and corners. A similar system was proposed in [20,21], where a smartphone was used to emit short 21.5 kHz pulses detected by an array of four microphones. This centralized system achieved errors below 10 cm by minimizing a positioning cost function. A different proposal was carried out in the *BeepBeep* ranging system [22], in this work the authors developed a two-way sensing technique to estimate the relative distance between a PDA and a smartphone. By measuring the ToA of chirp signals with frequencies between 2 and 6 kHz emitted by these devices, this system achieved positioning errors of 5 cm for distances below 4 m. Later, several works benefited from the *BeepBeep* ranging technique to develop different relative indoor positioning systems among smartphones and tablets [23,24], reporting average positioning errors between 10 and 30 cm. The main constraint of all these systems is their low update rate and low multi-user capability, in order to avoid signal collisions.

The current signal processing capabilities of smart mobile devices [25] allow for more efficient Code Division Multiple Access (CDMA) based systems, in which all signals can be emitted at the same time. The advantages of the CDMA scheme are well known and have been widely used in the design of general-purpose Ultrasonic Local Positioning System (ULPS) [26]. Also works like [27,28] have demonstrated the viability of using spread spectrum audible signals in a general-purpose ALPS using a set of four pseudorandom noise sequences and obtaining errors below 10 cm for 95% of measurements in a testing area of $6\times7\ m^2$. Unfortunately, the use of longer and simultaneous emissions in CDMA schemes comes hand in hand with the appearance of phenomena such as Multiple Access Interference (MAI) and Inter Symbol Interference (ISI) [29]. Due to the above mentioned audio system limitations, the implementation of a CDMA-ALPS with mobile devices either requires the use of an ultrasonic external acquisition system [30] or the emission of audible signals [31]. In this latter work, the authors presented a CDMA-ALPS for mobile devices using audible signals. This system was based on the use of four 255-bit Kasami codes, BPSK modulated at 20 kHz, which were acquired and match-filtered directly by an iPad in order to calculate its own position by means of multilateration. This system was evaluated in a $5.5\times5.75\ m^2$ positioning area obtaining errors below 10 cm for 70% of measurements at testing points free of MAI, ISI or multipath. These errors increased up to 90 cm at locations where these phenomena appear.

This work presents a new CDMA-ALPS which performs indoor localization of smartphones and tablets providing robust ToA estimations by using a MAI/ISI compensation algorithm. The system is based on the prototype presented by the authors in [31], where a similar architecture was proposed. However, this prototype lacked of several design aspects and signal processing tasks that severely reduced its performance, making it useless in a practical situation. The main improvements included in this evolution can be summarized as follows:

- Beacon locations are now determined using a metaheuristic search, in order to minimize the mean Position Dilution of Precision (PDOP) [32] in the entire location area.
- The temporal and spectral features of the emissions have been modified to reduce the effects of multipath and Doppler shift, as well as to minimize the losses caused by the receiver's microphone. These modifications are explained in detail in Section 2.2.
- A new algorithm has been implemented to avoid ambiguity between signals belonging to consecutive emissions.
- A MAI/ISI compensation algorithm has been implemented, completely redesigning the programming flow of the algorithm previously developed for a general purpose computer [29].

The next section of this paper presents a complete description of the ALPS, including design aspects, physical properties of the transducers and electronics, CDMA processing algorithms and programming. Section 4 contains the experimental evaluation of the positioning system, paying special attention to its performance with respect to MAI outliers rejection and noise addition. In Section 5 these results are discussed and further improvements of the system are pointed out. Finally, the most important conclusions of this work are drawn in Section 6.

2. Description of the acoustic local positioning system

The description of the ALPS proposed in this work is depicted in Fig. 1. As shown, Fig. 1(a) displays a picture of the location scenario where four acoustic emitting beacons are placed in a restricted volume inside of a box-shaped room, whose dimensions are detailed in Fig. 1(b). These beacons are close to the wall which is farthest from the entrance to the room and with their acoustic axis arranged perpendicular to it, thus allowing optimal signal reception to those users facing this wall. This configuration is particularly useful for certain types of LBS such as those designed to provide information to the visitors of a museum whose exhibits are shown in a single wall, as long as there are no occlusions of the direct propagation path.

On the other hand, Fig. 1 (c) depicts the PDOP values generated from the optimal beacons distribution obtained with the help of a Genetic Algorithm (GA). This algorithm was programmed to minimize the average PDOP value on the whole location area at 1.1 ± 0.2 meters height, starting with an initial population of 50 real-coded random emplacements for the beacons inside the beacon's location volume (see Fig. 1 (b)). A single-point crossover probability of 0.7 and mutation rate of 0.01 were defined, together with a tournament selection method, to meet a fitness stability convergence criteria within hundred generations.

The beacons are synchronized between themselves to emit four encoded acoustic signals that are detected with an unknown time base from the receiver (an iPad). The iPad identifies the received signals by correlation and obtains the Time-Differences-of-Arrival (TDoAs) between a reference beacon and the remaining ones. Finally, from these TDoAs the iPad computes its position by using multilateration.

The following subsections provide detailed information about the most relevant aspects of this ALPS, namely, the emitting and receiver transducers and their associated electronics, the acoustic positioning signals, the CDMA signal processing method for ToA estimation, the positioning algorithm, and the real time implementation of these algorithms in the iOS mobile platform.

2.1. Emitter and receiver architecture

The emission architecture is illustrated with the help of Fig. 2. The coded signals are synthesized using a Virtex 5 FPGA-based board [33], which has been programmed to simultaneously generate pseudorandom emissions every 80 ms. These digital signals are passed through two double digital-to-analog converter modules (Digilent PmodDA2 [34]), and then high-pass filtered to remove the DC offset.

Finally, they are fed to a pair of two-channel audio amplifiers (Philips TDA8920BTH [35]) powered with a DC source in order to drive a set of four speakers, see Fig. 3(a). Fig. 3(b), and (c) show respectively the acoustic directivity pattern and frequency response of the speakers, as provided by the manufacturer (Visaton CP13 [36]).

As stated before, the receiver module of the ALPS proposed in this work is an iOS device, particulary we have used a third generation iPad [37]. The acoustic signal containing the positioning codes emitted by the beacons is detected by the built-microphone of this device and then processed by its internal processor (A8X). Fig. 3 (d) shows the frequency response of this microphone, experimentally obtained in our laboratory (blue dots).

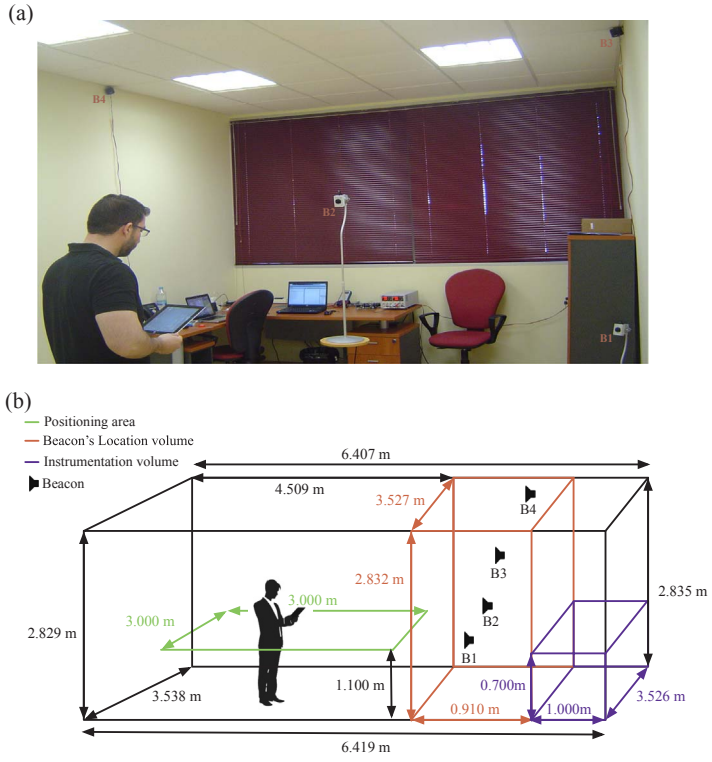

Fig. 1. Actual arrangement (a), dimensions of the location environment (b) and PDOP values and optimal beacons distribution (c). Beacon coordinates are measured with ± 1 mm accuracy by using a laser rangefinder (Bosch GLM80).

2.2. Positioning signals

In order to identify each beacon individually, their positioning signals are encoded with a unique, Binary-Phase Shift Keying (BPSK) modulated, pseudorandom Kasami code. These pseudo-orthogonal signals feature good aperiodic correlation properties [38] and Doppler effect tolerance [39], and for these reasons they are commonly used in matched filtering-based sonar systems [40–42]. We address now the choice of two key parameters: carrier frequency and code length of the positioning signals.

The carrier frequency (f_c) must lie within the combined bandwidth of the emitter and the receiver (2–20 kHz approximately), and it has been chosen as high as possible as to avoid causing excessive acoustic disturbance to normal human activity, but low enough as to maintain a

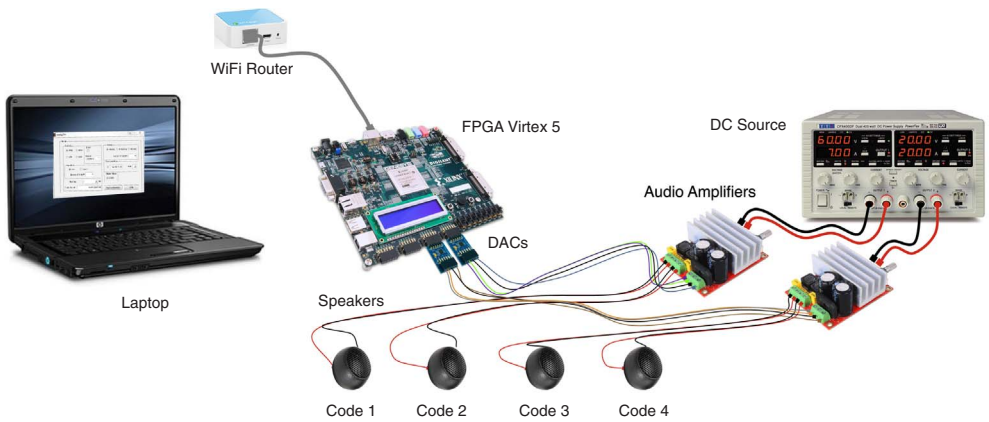

Fig. 2. Connection diagram of the emission architecture of the ALPS.

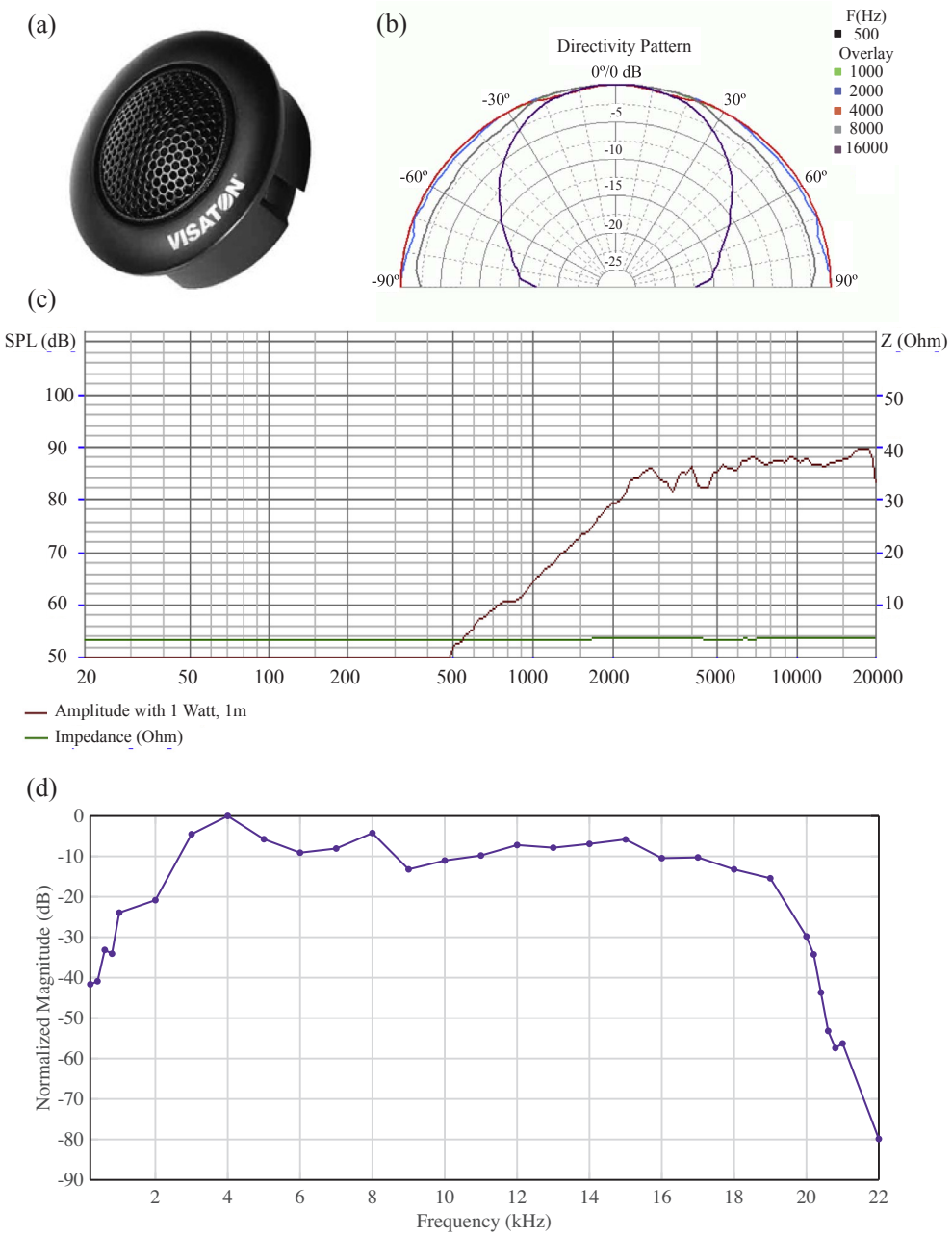

Fig. 3. Picture (a), directivity pattern (b) and frequency response (c) of the CP13 Visaton speaker, as provided by the manufacturer [36]. Frequency response of the receiver module (iPad's microphone) (d).

rather wide emission pattern. For that, we have chosen a carrier frequency of $f_c = 16$ kHz, with a root mean square (Gabor) bandwidth of 8 kHz. The spectral density of one of these signals is displayed in Fig. 4(a). On the other hand, Fig. 4(b) shows the high roll-off of the receiving system that eliminates 35% of the energy of the acoustic signal, however we found that the MAI/ISI compensation algorithm described later offered enough resilience and permitted to eliminate most of the outliers in the ToAs.

Regarding the Kasami code length, we experimented with 63 and 255 bits signals. Although longer codes provide larger correlation peaks, shorter codes are more Doppler tolerant (up to 1.5 m/s) [43] and more robust against multipath. Hence, we finally chose 63 bits Kasami codes, BPSK modulated with one cycle per bit.

To further study the effect on the ranging signals of the reduced bandwidth, we emitted a coded signal from a single beacon and received it with the iPad placed at a distance of 0.7 m, directly in front of it. Fig. 5 depicts the emitted and received signals, showing the filtering effects caused by the limited receiver's bandwidth. The aperiodic correlation of the received signal with the emitted code is shown in part (c), along with the ideal correlation. The degradation in the correlation shape, evidenced especially in the ringing after the first correlation peak, is due to the intersymbol interference (ISI) [44] caused by the limited bandwidth of the acoustic channel. This bandwidth limitation is more pronounced if the position of the receiver is far away from the axis of the emitter, due to the narrow directivity pattern of the emitter at high frequencies, shown in Fig. 5(b). Therefore, in order to provide robust Time-of-Arrival estimates for all beacons, CDMA signal processing must compensate these two effects: signal degradation due to limited bandwidth (ISI) and interference between all four emitting beacons (MAI). These aspects will be considered in the next section. Finally, Fig. 5(d) represents the crosscorrelation of the ideal and actual received signals with a different orthogonal code from the same Kasami family.

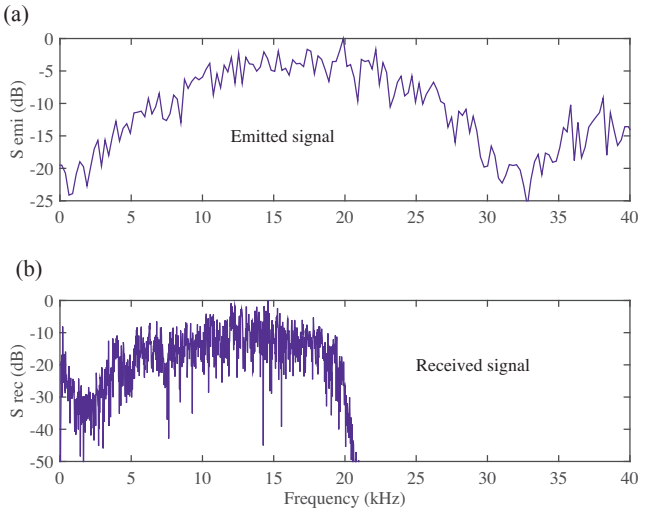

Fig. 4. Spectral density of emitted and received positioning signals, showing strong roll-off at 20 kHz.

2.3. CDMA signal processing

Determination of the ToAs of the different beacons from the acoustic signal received by the iPad can be achieved with a correlator bank [45]. However, this direct approach usually produces poor results, as it will be explained now.

The signal received by the microphone of the iPad is:

$$r(t) = \sum_{j=1}^{N} A_j \cdot (h_j * g_j)(t - t_j) + n(t), \tag{1}$$

where $N = 4$ is the number of acoustic beacons, $g_j(t)$ are the modulated coded signals, $\{t_j\}$ and $\{A_j\}$ are the ToAs and amplitudes of the signals to be estimated, $n(t)$ represents the noise, and index j runs from 1 to N. The effect on the signal of the acoustic channel is introduced in the convolution term $h_j(t)$. This represents the channel's impulse response and it is in principle unknown.

The output of the conventional receiver is formed by correlating $r(t)$ with all signal codes. For the k-th beacon:

$$R_{rg_k}(t) = A_k \cdot \underbrace{\left(h_k * R_{g_k g_k}\right)\left(t - t_k\right)}_{\widehat{\mathrm{ISI}}_k} + \underbrace{\sum_{j \neq k} A_j \cdot (h_j * R_{g_k g_j})(t - t_j)}_{\widehat{\mathrm{MAI}}_k} + \eta(t) \tag{2}$$

where $R_{g_k g_j}(t)$ is the cross-correlation of codes $g_k(t)$ and $g_j(t)$. As Eq. (2) outlines, there are two effects which deteriorate the estimation of the ToAs:

1. Intersymbol Interference (ISI), which is caused by the limited bandwidth of the acoustic channel (as we saw in Section 2.2), lowers the correlation peaks and degrades signal's detection and ranging.
2. Multiple Access Interference (MAI) between all the emitted codes in which larger amplitude signals difficult the detection of weaker signals emitted simultaneously; this is called the near-far effect [46].

Combined, both effects can lead to large deviations (outliers) of the ToA estimates from their true values.

Over time, a number of compensating alternatives for the effects of ISI and MAI interference have been devised [46]. The approach followed in this paper is based on a subtractive technique called Parallel Interference Cancellation (PIC) [29], in which the amplitude, delay, and impulse response of the signals from each beacon are estimated jointly, and the signals are re-encoded (with the proper amplitudes and delays) and subtracted from the received signal in order to get rid of MAI and ISI-caused disturbances.

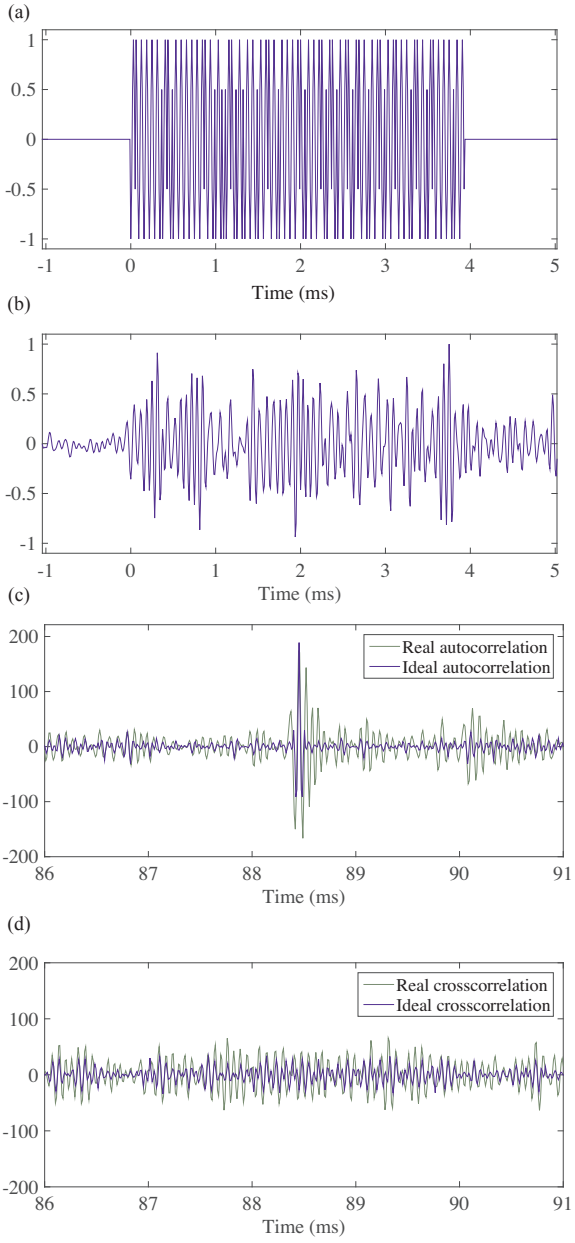

Fig. 5. Emitted (a) and received (b) signals, from only one beacon. Ideal versus real autocorrelation (c) and ideal versus real crosscorrelation (d) of the emitted codes.

The general scheme of the method adapted from [29] is shown in Fig. 6, and its steps are detailed now:

1. After the signal is acquired, initial estimates of amplitudes and ToAs are created by correlating $r(t)$ with the set of emitted codes $g_k(t)$. We have used parabolic interpolation in order to achieve subsample accuracy in both ToA and amplitude estimates [47]. For each beacon $k = 1...4$ we define the set $\mathscr{I}_j$ of values which represents the positions where the j-th beacon estimation component is subtracted from the received signal r(t). In the first step, $\mathscr{I}_j$ values range from L samples before the correlation peak sample to the correlation peak sample. Being L the number of samples of the j-th modulated code, in our case 378 samples.
2. The beacons are sorted in descending amplitudes, with more powerful beacons being processed first (this provides better immunity to near-far effects).
3. For the k-th beacon, we form signal $r_k(t)$ by subtracting the

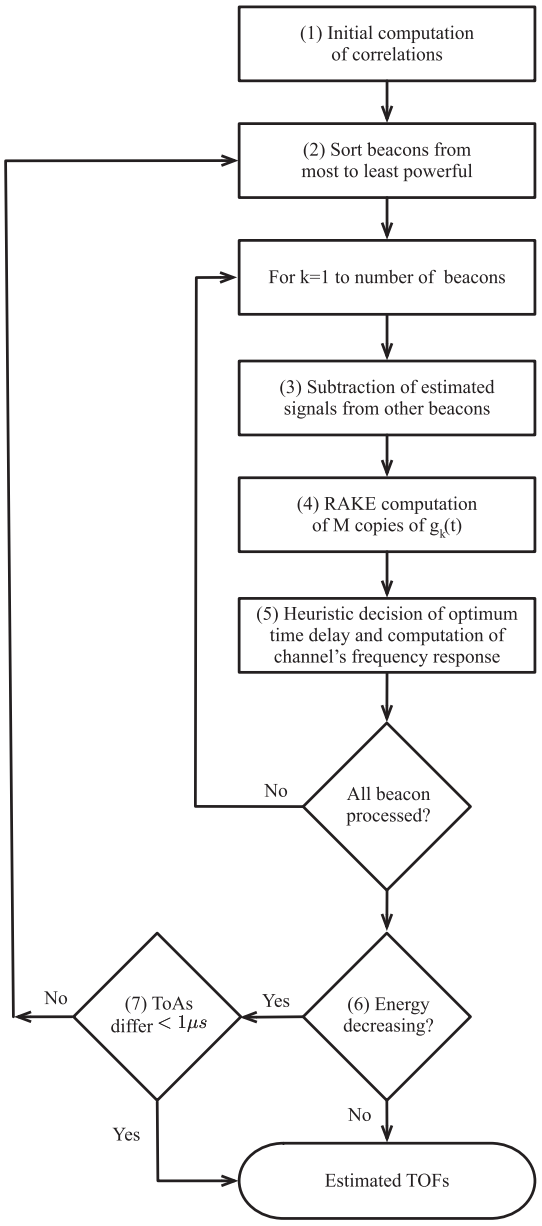

Fig. 6. Block diagram showing the flow of the subtractive parallel interference cancellation technique (adapted from [29]).

estimated components from all other beacons:

$$r_k(t) = r(t) - \sum_{\substack{j=1 \\ j \neq k}}^{N} \sum_{i \in \mathscr{I}_j} \widehat{A}_{ji} g_j(t - \hat{t}_{ji}), \tag{3}$$

where index i runs over a set of values $\mathscr{I}_j$. The signal $r_k(t)$ is the receiver's current best estimate of the k-th signal, without interference from other beacons.

4. We produce an array of M copies of $g_k(t)$ by repeatedly correlating $r_k(t)$ with the emitted code $g_k(t)$, and subtracting the estimated signal. In the context of channel estimation, this is similar to a RAKE receiver, and the copies of the emitted signal are called fingers [48]. Some of these fingers correspond to the frequency response of the k-th beacon, while others may be caused by not completely eliminated interference from the remaining beacons.
5. Among the set of M computed copies of $g_k(t)$, we must choose one as the most likely value for the actual k-th ToA. A heuristic criterion that gives good results consists in maximizing the product of the similarity of the finger's decoded signal and the emitted code g_k, multiplied by the finger's amplitude. Next, we consider that those signal's copies that arrive either too early before or too late after the correct one, are originated by noise or MAI from other beacons, and discarded.

The remaining set of copies (denoted as $\mathscr{I}_k$) are taken as the estimate of the impulse response of the k-th beacon:

$$A_k \cdot (h_k * g_k)(t) \simeq \sum_{i \in \mathscr{I}_k} \widehat{A}_{ki} g_k(t - \hat{t}'_i). \tag{4}$$

6. This action is repeated until all beacons have been processed, and then iteratively from step 2 above. The loop finishes when the energy of the residual signal obtained by subtracting all codes and all signal copies from the received signal stops decreasing, or when the ToAs differ by less than 1 μs from those computed in the previous iteration. This guarantees quick convergence of the iterative method.

2.4. Estimation of the receiver's position

Once the processor produces valid ToAs from the respective beacons (although referred to an unknown time base), hyperbolic multilateration is used by the receiver to estimate its position [49]. This technique involves measuring the TDoA between the first detected signal, emitted by the nearest beacon (BN) and the other signals detected subsequently, emitted by the remaining beacons. The locus of the points that measure the same TDoA between the nearest beacon and a second one (B1) define a hyperboloid whose focal points are those beacons. A second hyperboloid intersecting the first one can be obtained from the TDoA between the closest beacon and a third one (B2). With the help of a fourth beacon (B3), an additional hyperboloid intersecting the previous two in a single point can be obtained to fully determine the user's position. Fig. 7 shows a 2D representation of the multilateration technique.

The user's position can be obtained algebraically either by solving a system of nonlinear equations with four beacons or solving a system of linearized equations obtained by adding an extra beacon. However, in both cases, small errors in the differential distances measurements

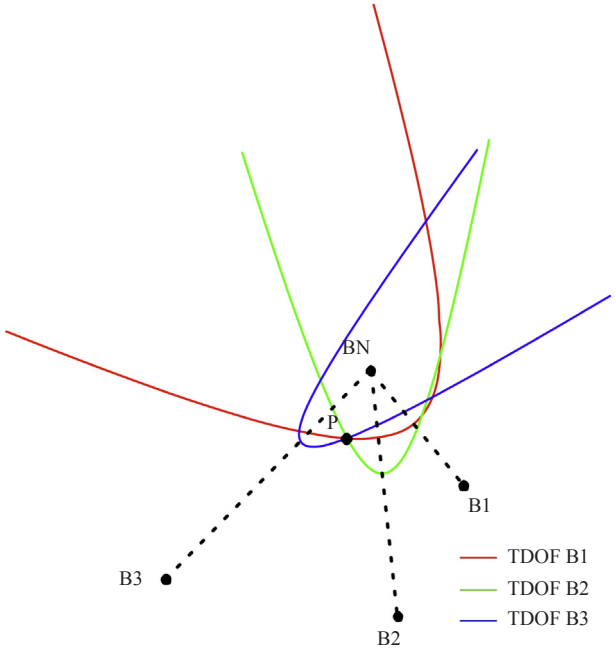

Fig. 7. Planar representation of the multilateration technique.

could cause important errors in the final position.

Our alternative here is to use the Gauss-Newton optimization algorithm to iteratively resolve the position as a non-linear least squares problem [50], providing greater robustness without adding any new beacon, at the expense of increasing the computational complexity. If we define the differential distance between beacon $\mathbf{b_i} = (x_i,y_i,z_i)$ and the nearest beacon $\mathbf{b_n} = (x_n,y_n,z_n)$ from the estimated user's position $\mathbf{p} = (x,y,z)$ as,

$$\hat{\Delta}r_i(\mathbf{p}) = \|\mathbf{b_i}-\mathbf{p}\|-\|\mathbf{b_n}-\mathbf{p}\| \quad \text{for } i = 1,2,3. \tag{5}$$

and the same distances obtained from the measured TDoAs as,

$$\Delta r_i = c\cdot \mathrm{TDoA}_i. \tag{6}$$

then we can build the objective function to be minimized as,

$$F(\mathbf{p}) = \sum_{i=1}^{3} [f_i(\mathbf{p})]^2 \tag{7}$$

where $f_i(\mathbf{p}) = \hat{\Delta}r_i(\mathbf{p})-\Delta r_i$.

Starting from an initial estimation of the position $\mathbf{p_0} = (x_0,y_0,z_0)$, subsequent estimates of this parameter can be obtained by means of the recursive relation:

$$\mathbf{p_{k+1}} = \mathbf{p_k}-\mathbf{J_f}(\mathbf{p_k})^{-1}\mathbf{f}(\mathbf{p_k}) \tag{8}$$

where $\mathbf{f}(\mathbf{p_k}) = (f_1,f_2,f_3)$ and $\mathbf{J_f}(\mathbf{p_k})$ is the Jacobian matrix of $\mathbf{f}$ with respect to $\mathbf{p_k}$, i.e.,

$$\mathbf{J_f}(\mathbf{p_k}) = \begin{pmatrix} \frac{\partial f_1}{\partial x} & \frac{\partial f_1}{\partial y} & \frac{\partial f_1}{\partial z} \\ \frac{\partial f_2}{\partial x} & \frac{\partial f_2}{\partial y} & \frac{\partial f_2}{\partial z} \\ \frac{\partial f_3}{\partial x} & \frac{\partial f_3}{\partial y} & \frac{\partial f_3}{\partial z} \end{pmatrix} \tag{9}$$

Subtractive techniques are not expected to provide perfect interference cancellation, especially in low Signal-to-Noise Ratio (SNR) situations (as we will consider in Section 4.2). Since our positioning system operates without time synchronization (hyperbolic multilateration) and uses exactly the minimum required number of beacons, ToA outliers cannot be detected by redundancy techniques (like the parity space [51]). Instead, we have implemented a straightforward method based in a temporal filter which discards ToA values which deviate largely from previously determined ones. Although simple, this technique permits to eliminate most instances of outliers in computed position.

3. Implementation in the mobile device

The implementation has been performed on a last generation iPad (iPad Air 2), which is equipped with 2 GB of LPDDR3-type RAM and a 32-bit processor (model APL1012). This processor, called A8X, features a triple-core CPU at 1.5 GHz (Cyclone 2nd generation) with an ARMv8-A instructions set. The processes of data acquisition, signal processing (correlation + MAI/ISI compensation), Gauss-Newton positioning computation and display of the results have been programmed in an Objective-C application with a total size of 1.3 MB. Approximately one third of this size (413 kB) corresponds to the MAI/ISI compensation algorithm, that takes 80 ms on average and 223 ms maximum to process the signals acquired in the buffer length. This algorithm has been set up to perform a maximum of 10 iterations obtaining 5 fingers per beacon in each iteration. This configuration produces a 90% probability of convergence before the fourth iteration. The operating block diagram of showing all the processes involved in the positioning app is represented in Fig. 8.

Digital acquisition of an audio signal with an iOS device requires the configuration of the *Audio Queue Services*, which is a C programming interface in *Core Audio Toolbox* framework, available through *The Mac Developer Library* [52]. The audio signals' acquisition rate was set to the maximum allowed by the iPad's hardware (96 kHz), although this results in a relatively low sampling/ carrier frequency ratio ($f_s/f_c = 6$). The buffer size was set to 8058 samples, so that every 84 ms the program saves data from the buffer to a pointer in memory. The length of the signal acquisition window corresponds with the length of two consecutive coded signal emissions (code + gap + code), which guarantees that the beacon ranging signal, will be captured entirely inside the buffer at least once.

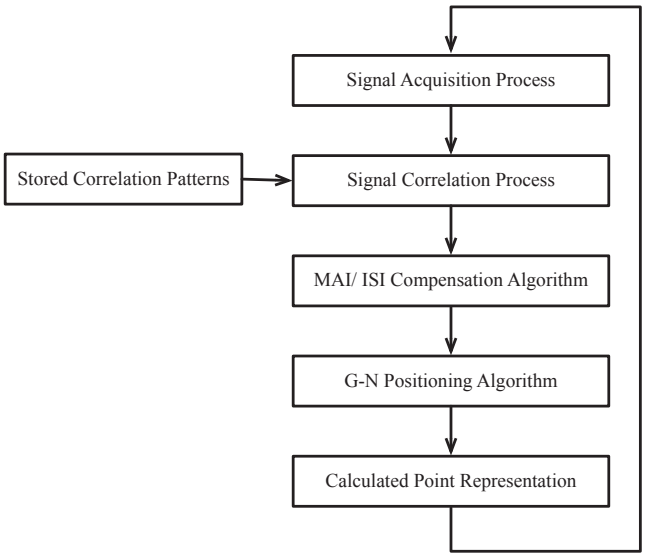

Fig. 8. Block diagram of the whole iOS positioning app.

After that, these samples are processed by means of the *vDSP API* which provides mathematical functions for applications involving data processing. The existence of an API that facilitates signal processing tasks was a key reason to choose iOS devices as the development platform for the implementation of the system.

After data acquisition and all processing tasks, the calculated position is displayed to the user. The developed user interface, whose screenshot is illustrated in Fig. 9, shows the plan of the room, the

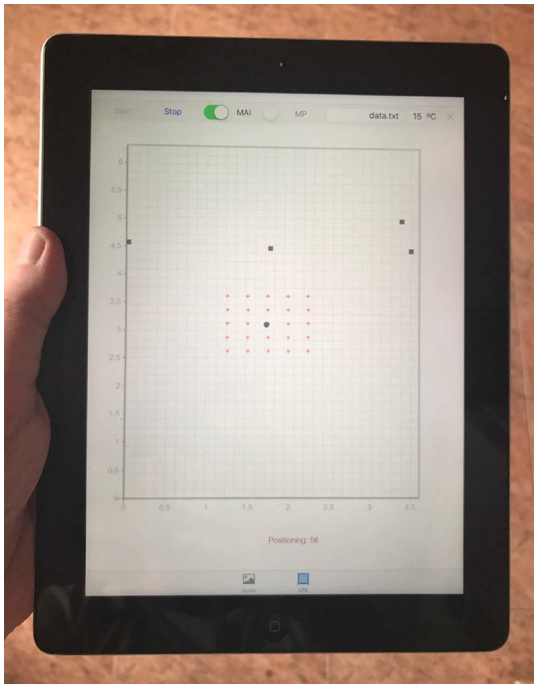

Fig. 9. Screenshot of the developed user interface.

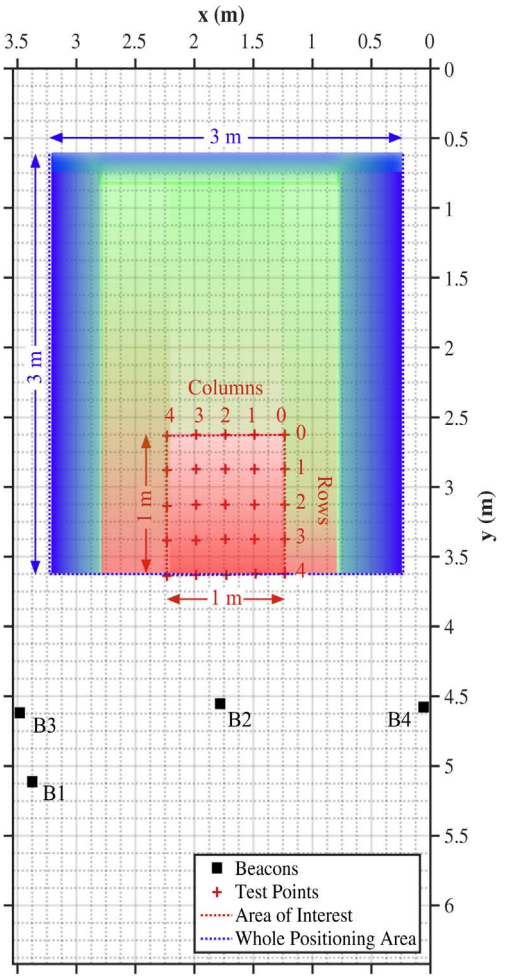

Fig. 10. Test points, beacon's location and positioning areas.

location of the beacons (black squares), the test points (red crosses) and the estimated position of the user (black circle) at every moment. Also, a text field for the filename where data are stored is included. Finally Start, Stop and Exit buttons are included to handle the application.

4. Experimental results

In this section, experimental results from the different tests carried out to evaluate the proposed system are presented. In these tests, a comparison between results obtained before and after the application of the MAI/ISI algorithm is conducted. Besides, the system performance when different levels of white Gaussian noise are added to the emitted signals is also studied. Experimental tests have been carried out in a box shaped room with low acoustic absorption and whose dimensions have been specified in Fig. 1(b). Inside this room, the LPS is designed to work in a square area of $3 \times 3\ m^2$ offering positioning errors below 10 cm in those locations far from walls and beacons (greenish area in Fig. 10). These errors rise above 20 cm when the receiver is close to a wall (bluish area in Fig. 10) due to the strong multipath effect. Even worse, the proximity of beacon 2 to the location area generates a strong MAI in its surroundings making the system useless in this zone (reddish area in Fig. 10). This work is focused on solving this later problem, and for this reason the area of interest has been reduced to a mesh of $1 \times 1\ m^2$ with 25 cm of resolution just in front of beacon 2. In total, a set of 25 test points (p_{ij}) have been specified according to their *i*-th row and *j*-th column at the locations depicted in Fig. 10. For each test point measured with the laser rangefinder and marked on the floor, the iPad's microphone has been placed on its vertical at 1.1 meters height with the help of a tripod and a plumb-line.

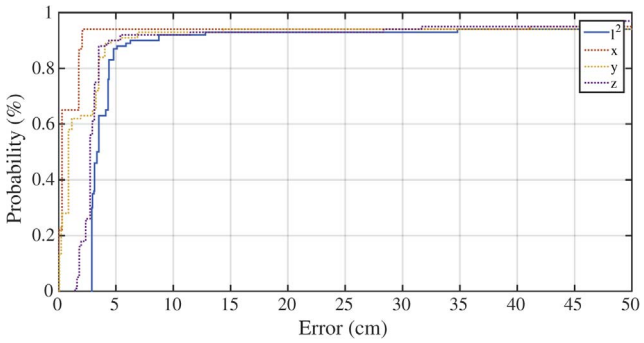

Fig. 11. Results with the user presence.

4.1. User's body echoes

The first experiment that has been carried out is checking the effects that the user's presence has on the results. To verify the existence of these possible effects two experimental tests (with and without the user presence) are performed, obtaining in each case a set of a hundred measurements at the center of the area of interest (p22). In both cases TDoA are obtained using simple correlation and the measured environmental temperature is 17.1 °C.

In a second experiment, the iPad's app was modified to start five seconds later the acquisition process, which is enough for the user to leave the room until the acquisition is completed. After data processing, positioning errors are represented by means of two Cumulative Distribution Function (CDF) graphs.

Fig. 11 shows the results obtained in p22 with the user presence. In this figure, positioning errors committed in x, y and z coordinates are represented as red, yellow and purple dashed lines respectively. Besides, the Euclidean norm of the total error $l^2 = \sqrt{x^2 + y^2 + z^2}$ is depicted as a solid blue line.

Figs. 12 shows the results obtained without the user presence, which are practically identical to those presented in Fig. 11, with errors below 5 cm for 85% of the measurements. From these results, it can be concluded that the user's presence does not have a significant effect on the system performance. From now on, all measurements will be carried out with the user's presence as befits a normal use of the iPad.

4.2. Performance and dependence with SNR

As stated before, the system proposed in this work has been designed to operate without time synchronization, and a hyperbolic positioning method is used. As the system has only four beacons, the presence of a single outlier in any of the ToAs in a given time slot renders the system useless for positioning. Two parameters have been considered to evaluate the performance of the system, namely, the

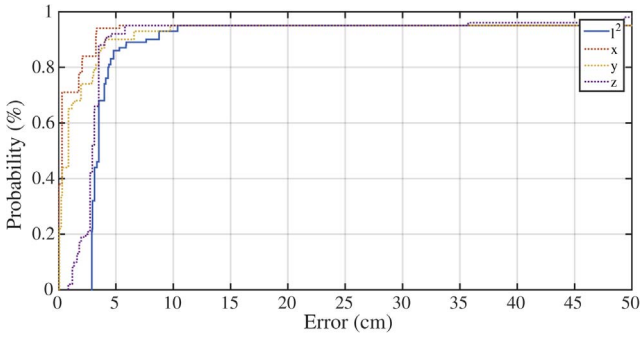

Fig. 12. Results without the user presence.

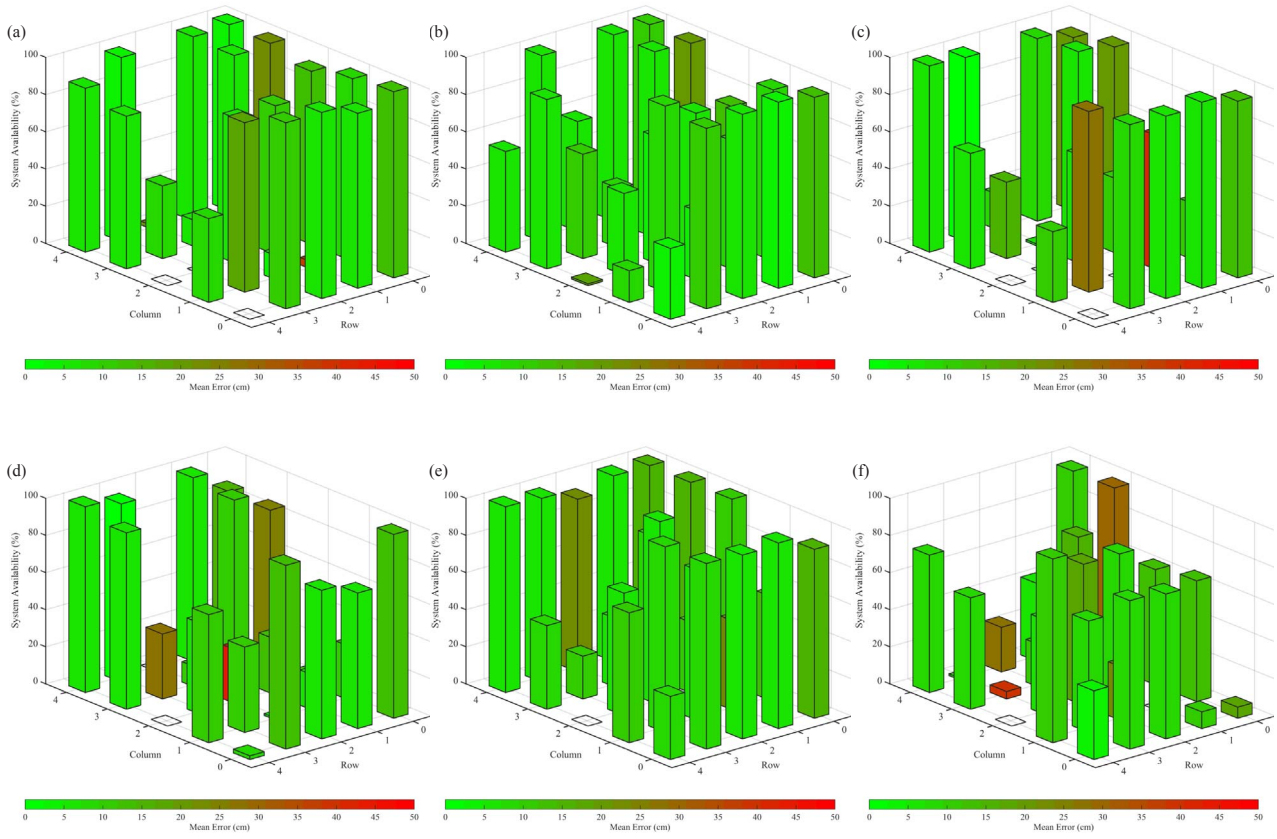

Fig. 13. Results applying simple correlation: (a) without added noise, (b) SNR 12 dB, (c) SNR 9 dB, (d) SNR 6 dB, (e) SNR 3 dB and (f) SNR 0 dB.

mean error committed in positioning and the System Availability (SA), defined as the percentage of measurements whose error is below the outliers threshold (50 cm).

For each one of the 25 test points defined above, a hundred of acquisitions of the received signal have been performed and later processed to obtain their corresponding ToA, first by simple correlation and second by applying the MAI compensation algorithm. From these ToAs a hundred estimations of the iPad's position have been calculated in each case, and from them, the mean error and the SA for each test point have been obtained. The SA at each test point is represented in the z-axis and the mean error committed is depicted using a color code. Hence, a good result (high SA with low error) corresponds to a long greenish bar, whereas a bad result (low SA with high error) is represented by a short reddish bar. Also, we have investigated the effect of noise on the system performance by adding white Gaussian noise to the emitted patterns to obtain Signal-to-Noise ratios of 12, 9, 6, 3 and 0 dB.

4.2.1. Simple correlation

Fig. 13 a) presents the mean error and the SA when no Gaussian noise is added to the emitted signal. This figure shows how those points near to beacon 2 (row 4) have the worst results. According to Fig. 10, B2 is the closest beacon to the location area, and for this reason all points on its surroundings are the most affected by Near-Far (NF) effect. This phenomenon is a type of MAI where the receiver captures a strong signal coming from B2 that makes it impossible to detect the weaker signals coming from the remaining beacons. It can be seen how test points p42, p40, p32, p21, p23 and p24, are the most affected by this phenomenon, with a SA close to zero and mean errors that can rise above 20 cm. There are also other points less affected by MAI such as p41 and p33 where the SA is around 40% with mean errors below 10 cm. The remaining test points present good results with a SA always above 80% and mean errors below 10 cm, except points p31, p00 and p02 that present a slightly larger error.

Also, Fig. 13(b), (c), (d), (e) and (f) show the results when emissions with SNRs of 12, 9, 6, 3 and 0 dB are considered respectively. As can be seen, as the SNR of the emitted signals decreases, the SA of those points affected by MAI also decreases and the corresponding positioning error increases. Conversely, in those test points where good results are obtained in the absence of noise the system performance is more robust against a decrease in the SNR.

4.2.2. MAI compensation technique

Next, the same acquired data have been processed using the MAI/ISI compensation algorithm. Fig. 14(a) represents the mean error and the SA without adding of Gaussian noise to the emitted signal. A clear improvement can be observed in these results with respect to those represented in Fig. 13(a), since now the SA for all test points is close to 100% with mean errors clearly below 10 cm.

Also, Fig. 14(b), (c), (d), (e) and (f) display results when emissions with SNRs of 12, 9, 6, 3 and 0 dB are used respectively. These figures show a clear improvement of the performance in noisy conditions when using the MAI/ISI cancellation algorithm. As expected, the average SA in the area of interest decreases with increasing noise, although high values of this parameter are obtained for SNR as low as 3 dB. Only in the last case considered, with SNR = 0 dB, a noticeable worsening of the results is observed. See, for example, the results obtained in this case in test points p00, p20, p22, p31 and p34, where the SA has dropped to values below 30%. In some of these points, such as p00 and p34, a slight increment of the mean positioning error is also detected. There are finally other test points, such as p02, p03, p11 and p21, that exhibit a moderate decrease of SA but with a significant worsening of the mean positioning error.

As an additional test to demonstrate the improved accuracy

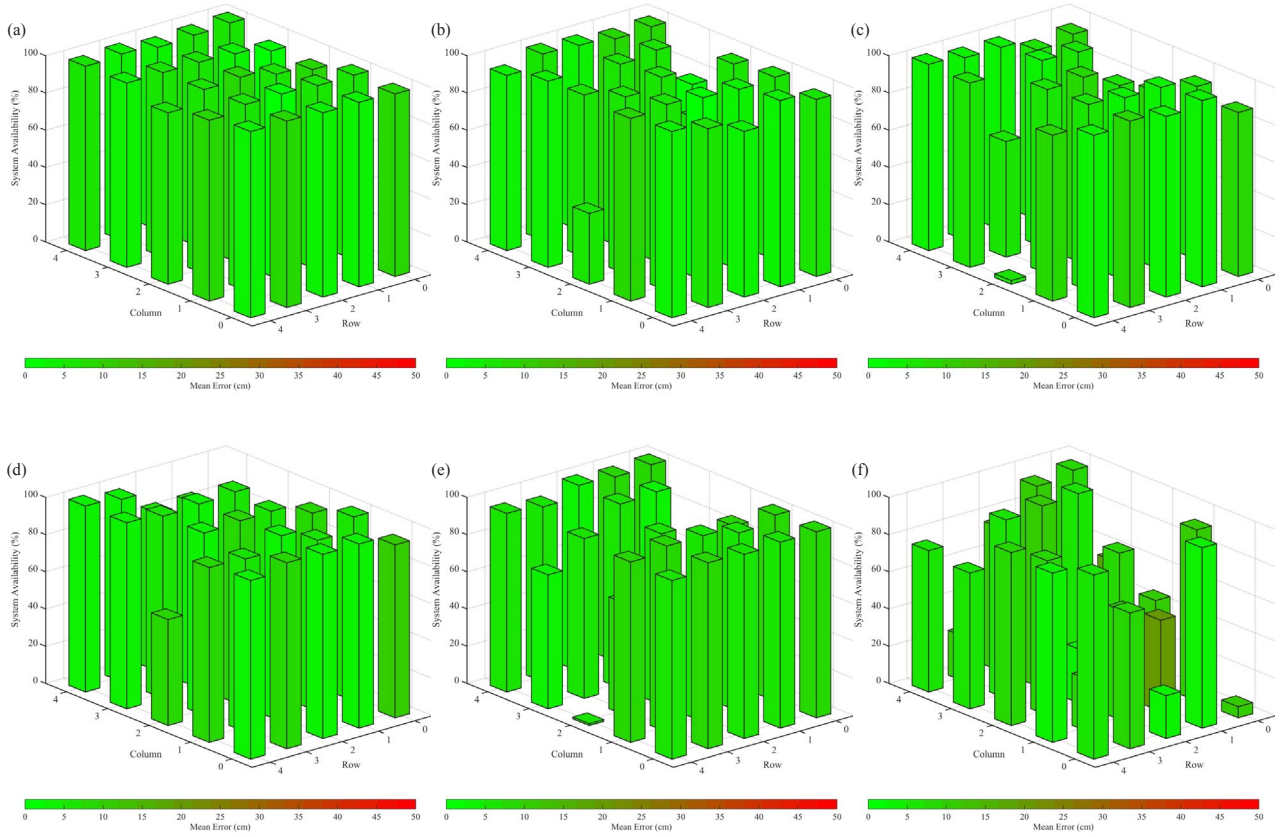

Fig. 14. Results applying MAI compensation: (a) without added noise, (b) SNR 12 dB, (c) SNR 9 dB, (d) SNR 6 dB, (e) SNR 3 dB and (f) SNR 0 dB.

achieved with the proposed algorithm, the iPad has been moved around the perimeter of the area of interest, handheld at a height of around 1.1 m above the floor.

Due to the influence that Doppler shift has on the shape of the received signals, this trajectory has been carried out at 0.5 m/s speed, thus avoiding errors caused by this phenomenon [43]. Also note that multipath has not a significant effect on the results since the chosen trajectory is far from walls. In this experiment no additional noise has been added to the emitted signals, and just a weak environmental noise (40 dB) is present. In total, 400 measurements have been acquired with the iPad along the entire trajectory. A room temperature of 17.4 °C has been measured at the beginning of the process that translates into a sound speed of 342 m/s used in range computations.

Fig. 15 shows the actual path (black solid line), the beacon's location (black squares) and the positioning results obtained along the entire trajectory, with (blue dots) and without (red dots) MAI/ISI compensation. As shown in this figure, without MAI/ISI compensation a significant number of outliers is obtained (positioning errors > 50 cm) which reduce the SA to 50%. These outliers can represent errors greater than 2 meters in some cases, revealing both a low system accuracy and a poor reliability under MAI conditions. However, after MAI/ISI compensation these results significantly improve, achieving a SA above 90% and positioning errors below 10 cm. These results are in concordance with the static results obtained in Fig. 14(a), showing that the system offers good performance and reliability in motion provided the speed of the receiver is not high enough as to cause a relevant Doppler shift.

5. Discussion

In the previous sections we have presented the design of an ALPS to gain accurate positioning within a room of small dimensions. This system operates with the minimum number of beacons (4) necessary to ensure positioning by using hyperbolic lateration, and proposes the use of a commercial mobile device as the receiver module. It was among the aims of this work to demonstrate that it is possible to get accurate positioning from a minimal deployment of beacons by using a mobile device off-the-shelf. As it is well known, this kind of devices suffers from a significant lack of performance in advanced processing tasks and a limited bandwidth microphone. However, our system provides similar precision (errors below 10 cm) and update rate (> 2 Hz) than other general-purpose CDMA-based ultrasonic LPS that use a broad bandwidth microphone and specifically designed hardware for the receiver module [53,54].

Although the system presented in this work is intended to cover a $3 \times 3\,m^2$ area, it could be extended by using several clusters of five beacons, where each one of them differs from the rest in single beacon (the cluster identifier) and cover a particular area of the total working area. Besides, to assist location in uncovered areas, an auxiliary PDR system based on the portable device's accelerometer and gyroscope could be used. This architecture minimizes the number of different beacons to be identified and thereby reduces the computational cost. This approach has been already proposed in [55] for a mobile robot that uses odometry to navigate between nearby clusters.

It is important to remark that the system presented in this work has been specifically designed to tackle the problem of Multiple Access Interference that characterizes CDMA-based systems. Other phenomena that can have a major influence on the performance of an acoustic system have been deliberately avoided. This is, for example, the case of Doppler shift caused by the movement of the receiver that has been investigated by the authors in the past [39,43]. From these previous studies it is known that the proposed emissions are still detectable at receiver velocities up to 1.5 m/s, which is a reasonable upper limit when the receiver is being carried by a person. Another important

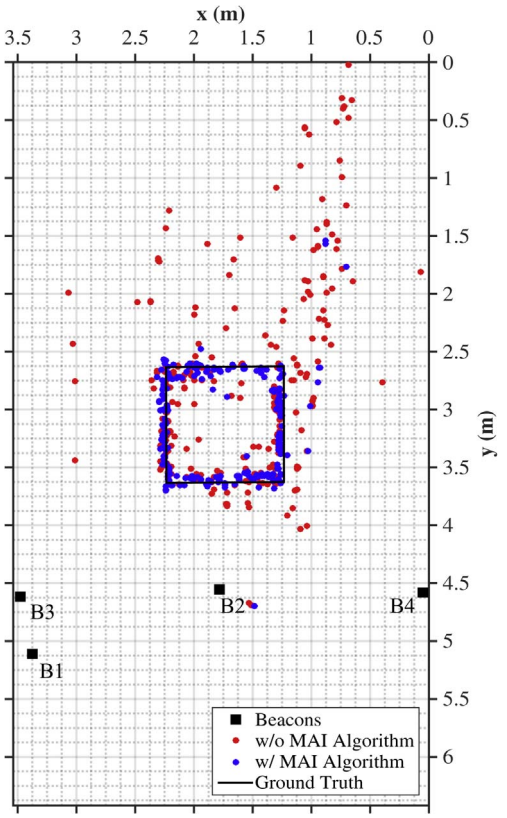

Fig. 15. Results obtained with (blue dots) and without (red dots) using the MAI cancellation technique respect the actual trajectory (black line). (For interpretation of the references to color in this figure legend, the reader is referred to the web version of this article.)

phenomenon is multipath, whose effect has been minimized in this work by installing the system in an empty room and establishing the area of interest in a region away from the room walls. Finally, environmental temperature is also a parameter that deserves some consideration in airborne acoustic systems, since it has a relevant influence on sound speed. In this work an homogeneous temperature distribution has been assumed, further evolutions of the proposed system may incorporate a network of temperature sensors strategically distributed around the environment from where a more realistic temperature distribution could be modeled and used to enhance the system accuracy.

It is also worth mentioning that the audible transient effects produced between emissions should be considered in a final commercial version of this system. These sounds cause a relatively small increment of 7 dB (from 40 to 47 dB) in the A-weighted room noise level that we all agree, even the youngest author, to consider largely bearable. A similar perception was expressed by the authors in [27] when comparing three different multiple access methods in a audible sound LPS. However, we share with these authors the opinion that a detailed psychoacoustic study with a wider target population would be required to assess the annoyance factor and other metrics.

Finally, note that the field of mobile devices is constantly evolving and provide shorter and shorter processing times. This will allow the implementation of more complex processing tasks to improve the performance of the MAI/ISI algorithm, as for example the use of the more efficient GCC-PHAT correlation function proposed in [27].

6. Conclusions

This work describes an acoustic local positioning system (ALPS) suitable for indoor positioning of portable devices such as a smartphone or a tablet computer, and based on the transmission of high frequency, CDMA-coded signals from a fixed beacon network to a mobile device. The system permits localization of the device (and the user carrying it) with enough accuracy for most Location-Based Services (LBS) in places such as museums, airports and malls. The most remarkable novelties of our ALPS are its feasibility to be implemented on smartphones and tablets (the user only needs to download and install the app) and its capability to use a CDMA scheme for localization, including MAI/ISI compensation techniques which mitigate range measurement degradation and the multiple access interference between the different beacons. The ALPS has been implemented in an smart device in order to take advantage of its hardware and processing performance. Signal reception, processing and estimation of position all take place within the tablet computer, operating at real time and with a position update of 2 Hz. It is important to remark that, although the detection application has been implemented in an iOS based platform, its extension to other mobile platforms such as Android or Windows Phone is feasible with some minor changes relative to the programming languages.

Experimental results show that the ALPS works successfully in indoor environments, eliminating most MAI/ISI effects and it is able to produce a position estimate with accuracy of 10 cm for 90% of the measurements in the region of interest. Also, the MAI/ISI algorithm has demonstrated to be robust against noise allowing reliable positioning with SNR levels as low as 3 dB.

Acknowledgments

This work was supported by the Spanish Ministry of Economy and Competitiveness (TARSIUS project, Ref. TIN2015-71564-C4-2/4-R), the Regional Government of Extremadura through the European Regional Development Funds (GR15167) and the Spanish Thematic Network on Indoor Positioning and Indoor Navigation, REPNIN (TEC2015-71426-REDT).

References

[1] H. Liu, H. Darabi, P. Banerjee, J. Liu, Survey of wireless indoor positioning techniques and systems, Systems, Man, and Cybernetics, IEEE Trans. Part C: Appl. Rev. 37 (6) (2007) 1067–1080.
[2] R. Mautz, Indoor Positioning Technologies, Institute of Geodesy and Photogrammetry, Department of Civil, Environmental and Geomatic Engineering, ETH Zurich, 2012.
[3] R.F. Brena, J.P. García-Vázquez, C.E. Galván-Tejada, D. Muñoz-Rodriguez, C. Vargas-Rosales, J. Fangmeyer, Evolution of indoor positioning technologies: a survey, J. Sens. 2017 (2017) 21, http://dx.doi.org/10.1155/2017/2630413 Article ID 2630413.
[4] R. Harle, A survey of indoor inertial positioning systems for pedestrians, IEEE Commun. Surv. Tutor. 15 (3) (2013) 1281–1293, http://dx.doi.org/10.1109/SURV.2012.121912.00075.
[5] A. Jiménez, F. Zampella, F. Seco, Improving inertial pedestrian dead-reckoning by detecting unmodified switched-on lamps in buildings, Sensors 14 (1) (2014) 731–769.
[6] F. Li, C. Zhao, G. Ding, J. Gong, C. Liu, F. Zhao, A reliable and accurate indoor localization method using phone inertial sensors, Proceedings of the 2012 ACM Conference on Ubiquitous Computing, UbiComp '12, ACM, New York, NY, USA, 2012, pp. 421–430, , http://dx.doi.org/10.1145/2370216.2370280.
[7] S. Subramanian, J. Sommer, S. Schmitt,W. Rosenstiel, Sbil: Scalable Indoor Localization and Navigation Service (2007) 27–30.
[8] S.P. Khare, J. Sallai, A. Dubey, A. Gokhale, Short paper: towards low-cost indoor localization using edge computing resources, in: 2017 IEEE 20th International Symposium on Real-Time Distributed Computing (ISORC), 2017, pp. 28–31. doi:http://dx.doi.org/10.1109/ISORC.2017.23.
[9] A.R.J. Ruiz, F.S. Granja, Comparing Ubisense, BeSpoon, and DecaWave UWB location systems: indoor performance analysis, IEEE Trans. Instrum. Meas. 66 (8) (2017) 2106–2117, http://dx.doi.org/10.1109/TIM.2017.2681398.
[10] Y. Zhuang, Z. Syed, Y. Li, N. El-Sheimy, Evaluation of two WiFi positioning systems based on autonomous crowdsourcing of handheld devices for indoor navigation, IEEE Trans. Mobile Comput. 15 (8) (2016) 1982–1995, http://dx.doi.org/10.1109/TMC.2015.2451641.
[11] Q. Chang, S. Van de Velde, W. Wang, Q. Li, H. Hou, S. Heidi, Wi-Fi Fingerprint Positioning Updated by Pedestrian Dead Reckoning for Mobile Phone Indoor Localization, Springer Berlin Heidelberg, Berlin, Heidelberg, 2015, http://dx.doi.org/10.1007/978-3-662-46632-2_63.
[12] T. Gallagher, E. Wise, B. Li, A. Dempster, C. Rizos, E. Ramsey-Stewart, Indoor positioning system based on sensor fusion for the blind and visually impaired, in: 2012 International Conference on Indoor Positioning and Indoor Navigation (IPIN),

2012, pp. 1–9.
[13] L. Pei, J. Liu, R. Guinness, Y. Chen, H. Kuusniemi, R. Chen, Using ls-svm based motion recognition for smartphone indoor wireless positioning, Sensors 12 (5) (2012) 6155–6175, http://dx.doi.org/10.3390/s120506155.
[14] W. Kang, Y. Han, SmartPDR: smartphone-based pedestrian dead reckoning for indoor localization, IEEE Sensors J. 15 (5) (2015) 2906–2916, http://dx.doi.org/10.1109/JSEN.2014.2382568.
[15] J. s. Jeon, Y. Kong, Y. Nam, K. Yim, An indoor positioning system using bluetooth RSSI with an accelerometer and a barometer on a smartphone, in: 2015 10th International Conference on Broadband and Wireless Computing, Communication and Applications (BWCCA), 2015, pp. 528–531. doi:http://dx.doi.org/10.1109/BWCCA.2015.142.
[16] A. Bahillo, J. Prieto, H. Fernández, P. Fernández, R. Lorenzo, E. Abril, Fusing Technologies for a Continuous Positioning Solution Developed on a Smartphone, in: 2012 7th International Conference on Computing and Convergence Technology (ICCCT), 2012, pp. 763–766.
[17] M.-H. Kang, B.-G. Lim, Development of a practical foolproof system using ultrasonic local positioning, Measurement 79 (2016) 1–14, http://dx.doi.org/10.1016/j.measurement.2015.10.010.
[18] A. Mandal, C. Lopes, T. Givargis, A. Haghighat, R. Jurdak, P. Baldi, Beep: 3D indoor positioning using audible sound, Consumer Communications and Networking Conference, 2005. CCNC. 2005 Second IEEE, 2005, pp. 348–353.
[19] C.V. Lopes, A. Haghighat, A. Mandal, T. Givargis, P. Baldi, Localization of off-the-shelf mobile devices using audible sound: architectures, protocols and performance assessment, SIGMOBILE Mob. Comput. Commun. Rev. 10 (2) (2006) 38–50.
[20] V. Filonenko, C. Cullen, J. Carswell, Investigating ultrasonic positioning on mobile phones, in: 2010 International Conference on Indoor Positioning and Indoor Navigation (IPIN), 2010, pp. 1–8.
[21] V. Filonenko, C. Cullen, J.D. Carswell, Indoor positioning for smartphones using asynchronous ultrasound trilateration, ISPRS Int. J. Geo-Inform. 2 (3) (2013) 598–620.
[22] C. Peng, G. Shen, Y. Zhang, Y. Li, K. Tan, BeepBeep: a high accuracy acoustic ranging system using COTS mobile devices, Proceedings of the 5th International Conference on Embedded Networked Sensor Systems, SenSys '07, ACM, New York, NY, USA, 2007, pp. 1–14.
[23] B. Xu, R. Yu, G. Sun, Z. Yang, Whistle: synchronization-free TDOA for localization, in: 2011 31st International Conference on Distributed Computing Systems (ICDCS), 2011, pp. 760–769.
[24] J.-W. Qiu, C.C. Lo, C.-K. Lin, Y.-C. Tseng, A D2D relative positioning system on smart devices, in: IEEE Wireless Communications and Networking Conf. (WCNC), 2014.
[25] A.J. Bianchi, M. Queiroz, On the performance of real-time DSP on android devices, in: Proceedings of the 9th Sound and Music Computing Conference, 2012, pp. 113–120.
[26] M.C. Perez, J. Urena, A. Hernandez, A. Jimenez, D. Ruiz, F.J. Alvarez, C.D. Marziani, Performance comparison of different codes in an ultrasonic positioning system using DS-CDMA, in: 2009 IEEE International Symposium on Intelligent Signal Processing, 2009, pp. 125–130. doi:http://dx.doi.org/10.1109/WISP.2009.5286574.
[27] J. Moutinho, R. Araújo, D. Freitas, Indoor localization with audible sound - towards practical implementation, Pervasive Mob. Comput. 29 (2016) 1–16, http://dx.doi.org/10.1016/j.pmcj.2015.10.016.
[28] J. Moutinho, D. Freitas, R. Esteves Araújo, Indoor global localisation in anchor-based systems using audio signals, J. Navig. 69 (5) (2016) 1024–1040, http://dx.doi.org/10.1017/S0373463315001095.
[29] F. Seco, J.C. Prieto, A.R.J. Ruiz, J. Guevara, Compensation of multiple access interference effects in CDMA-based acoustic positioning systems, IEEE Trans. Instrum. Meas. 63 (10) (2014) 2368–2378, http://dx.doi.org/10.1109/TIM.2014.2312511.
[30] M.C.Pérez, D. Gualda, J.M. Villadangos, J. Ureña, P. Pajuelo, E. Díaz, E. García, Android application for indoor positioning of mobile devices using ultrasonic signals, in: 2016 International Conference on Indoor Positioning and Indoor Navigation (IPIN), 2016, pp. 1–7. doi:http://dx.doi.org/10.1109/IPIN.2016.7743628.
[31] T. Aguilera, J.A. Paredes, F.J. Álvarez, J.I. Suárez, A. Hernández, Acoustic local positioning system using an iOS device, in: 2013 International Conference on Indoor Positioning and Indoor Navigation (IPIN), 2013, pp. 1–8.
[32] R.B. Langley, Dilution of precision, GPS World 10 (5) (1999) 52–59.
[33] Genesys Virtex-5 FPGA Development Board Datasheet, 2016. < http://www.digilentinc.com/Products/Detail.cfm?Prod=GENESYS > .
[34] Pmod Digital-to-Analog Coverter datasheet, 2016. < https://reference.digilentinc.com/_media/pmod:pmod:pmodDA2_rm.pdf > .
[35] Type-D Dual Channel Audio Amplifier, 2016. < http://www.classdaudio.com/amplifier-modules/all-modules/cda-224-audio-amplifier-60w-x-2-8-ohm-120w-x-2-4-ohm.html#product_tabs_additional_tabbed > .
[36] CP13 Visaton Speaker Datasheet, 2016. < http://www.visaton.com/en/car_hifi/ht_kalotten/cp13_4.html > .
[37] iPad Technical Specifications, 2014. < http://support.apple.com/kb/SP708?viewlocale=en_US&locale=en_US > .
[38] T. Kasami, Weigh Distribution Formula for Some Class of Cyclic Codes, Technical Report R-285.
[39] F.J. Álvarez, A. Hernández, J.A. Moreno, M.C. Pérez, J. Ureña, Doppler-tolerant receiver for an ultrasonic lps based on kasami sequences, Sens. Actuat. A: Phys. (2013) 238–253.
[40] H. Peremans, K. Audenaert, J.M.V. Campenhout, A high-resolution sensor based on tri-aural perception, IEEE Trans. Robot. Autom. 9 (1) (1993) 36–48.
[41] J. Ureña, M. Mazo, J.J. García, A. Hernández, E. Bueno, Correlation detector based on a FPGA for ultrasonic sensors, Microprocess. Microsyst. 23 (1999) 25–33.
[42] F.J. Álvarez, J. Ureña, M. Mazo, A. Hernández, J. García, C.D. Marziani, High reliability outdoor sonar prototype based on efficient signal coding, IEEE Trans. Ultrason. Ferroelectr. Freq. Control 53 (10) (2006) 1862–1872.
[43] J.A. Paredes, T. Aguilera, F.J. Álvarez, J. Lozano, J. Morera, Analysis of doppler effect on the pulse compression of different codes emitted by an ultrasonic LPS, Sensors 11 (11) (2011) 10765–10784.
[44] J.G. Proakis, Digital Communications, fourth ed., McGraw-Hill, 2000.
[45] S. Moshavi, Multi-user detection for DS-CDMA communications, IEEE Commun. Mag. 34 (10) (1996) 124–136.
[46] J. Andrews, Interference cancellation for cellular systems: a contemporary overview, Wirel. Commun. IEEE 12 (2) (2005) 19–29.
[47] I. Céspedes, Y. Huang, J. Ophir, S. Spratt, Methods for estimation of subsample time delays of digitized echo signals, Ultrason. Imag. 17 (2) (1995) 142–171.
[48] H. Meyr, M. Moeneclaey, S.A. Fechtel, Digital Communication Receivers, Synchronization, Channel Estimation, and Signal Processing, Wiley Interscience, 1997.
[49] W.H. Foy, Position-location solutions by Taylor-series estimation, IEEE Trans. Aerospace Electron. Syst. AES-12 (2) (1976) 187–194.
[50] A. Björck, Numerical Methods for Least Squares Problems, SIAM, 1996.
[51] M.A. Sturza, Navigation System Integrity Monitoring using Redudant Meaurements, J. Inst. Navig. 35 (4) (1988) 69–87.
[52] Xcode Software Development Kit (SDK), 2016. < https://developer.apple.com/xcode/ > .
[53] D. Ruiz, E. García, J. Ureña, J.M. Villadangos, J.J. García, C.D. Marziani, Performance comparison of correlation-based received filters in an ultrasonic indoor positioning system, in: 2014 IEEE International Instrumentation and Measurement Technology Conference (I2MTC) Proceedings, 2014, pp. 1548–1551. doi:http://dx.doi.org/10.1109/I2MTC.2014.6861005.
[54] A. Hernández, E. García, D. Gualda, J. Villadangos, S. Gutiérrez, F. Nombela, M. Pérez, J. Ureña, Flexible Ultrasonic Beacon Unit based on SoC for Local Positioning Systems, in: 2015 International Conference on Indoor Positioning and Indoor Navigation (IPIN), 2015, pp. 1–6.
[55] D. Ruiz, E. García, J. Ureña, D. de Diego, D. Gualda, J.C. García, Extensive Ultrasonic Local Positioning System for navigating with mobile robots, in: 2013 10th Workshop on Positioning, Navigation and Communication (WPNC), 2013, pp. 1–6. doi:http://dx.doi.org/10.1109/WPNC.2013.6533279.